J Mol Model (2007) 13: 29–41
DOI 10.1007/s00894-006-0117-z

ORIGINAL PAPER

Kelby B. Napier · Zi-xuan Wang · Stephen C. Peiper · John O. Trent

CCR5 interactions with the variable 3 loop of gp120

Received: 14 November 2005 / Revised: 13 March 2006 / Published online: 24 May 2006

Abstract The G-protein coupled receptor CCR5 functions pathologically as the primary co-receptor for macrophage tropic (R5) strains of HIV-1. The interactions responsible for co-receptor activity are unknown. Molecular-dynamics simulations of the extracellular and adjacent transmembrane domains of CCR5 were performed with explicit solvation utilizing a rhodopsin-based homology model. The functional unit of co-receptor binding was constructed via docking and molecular-dynamics simulation of CCR5 and the variable 3 loop of gp120, which is a dominant determinant of co-receptor utilization. The variable 3 loop was demonstrated to interact primarily with the amino terminus and the second extracellular loop of CCR5, providing novel structural information regarding the co-receptor-binding site. Alanine mutants that alter chemokine binding and co-receptor activity were examined. Molecular-dynamics simulations with and without the variable 3 loop of gp120 were able to rationalize the activities of these mutants successfully, providing support for the proposed model. Based on these results, the global complex of CCR5, gp120 including the V3 loop and CD4, was investigated. The utilization of computational analysis, in combination with molecular biological data, provides a powerful approach for understanding the use of CCR5 as a co-receptor by HIV-1.

Keywords HIV-1 · CCR5 · Molecular modeling · gp120 · V3 loop

Electronic Supplementary Material Supplementary material is available for this article at http://dx.doi.org/10.1007/s00894-006-0117-z

K. B. Napier · J. O. Trent
Department of Biochemistry and Molecular Biology,
University of Louisville,
Louisville, KY 40202, USA

Z.-x. Wang ·
S. C. Peiper
Department of Pathology and Institute of Molecular Medicine and Genetics, Medical College of Georgia,
Augusta, GA 30912, USA

J. O. Trent
J. G. Brown Modeling Facility, Brown Cancer Center,
University of Louisville,
Louisville, KY 40202, USA

J. O. Trent (✉)
Department of Medicine, University of Louisville,
Louisville, KY 40202, USA
e-mail: john.trent@louisville.edu
Tel.: +1-502-8522194
Fax: +1-502-8524311

Introduction

CCR5 is a member of the serpentine-receptor superfamily, whose physiological ligands include RANTES (CCL5), MIP-1α (CCL3), and MIP-1β (CCL4) [1]. This chemokine receptor is expressed by monocytes, memory T lymphocytes, and preferentially by Th1 cells and NK cells [2–4]. CCR5 functions as a co-receptor for macrophage tropic (R5) strains of HIV-1 [5, 6] by associating with the viral envelope glycoprotein gp120, leading to envelope fusion and viral entry [7–9]. Individuals who are homozygous for an internal 32-bp deletion in the gene encoding CCR5 produce a truncated form of the receptor that is not expressed on the cell surface, providing a high degree of resistance to M-tropic strains of HIV-1 [10, 11].

The physiological ligands of CCR5 have been shown to block the co-receptor activity of M-tropic HIV-1 [7, 12–14]. In contrast, the viral chemokine vMIP-II [15], a high affinity antagonist of CCR5, has been shown to have limited efficacy as an inhibitor of co-receptor activity [16]. This difference may be attributed to the binding of these ligands to different regions of CCR5, indicating the importance of the N-terminal extracellular region (N-ter) and the second extracellular loop (ECL2) in co-receptor activity [17, 18]. Both the N-ter and the body of CCR5 have been shown to effect the co-receptor activity of reciprocal chimeras of CCR5 [19]. A chimera in which ECL2 of human CCR5 inserted into the body of a co-receptor-inactive murine CCR5 was found to confer co-receptor activity for some R5 strains of HIV-1 [20].

Monoclonal antibodies recognizing epitopes in ECL2 have been found to block infection with greater efficacy than those directed against the N-ter [21, 22]. Synthetic peptides derived from the extracellular loops of CCR5, particularly ECL2, have been shown to inhibit HIV-1 co-receptor activity [20].

The importance of the N-ter domain has been shown in several studies, which implicate specific acidic and aromatic residues in co-receptor activity [23–25]. Replacement of the N-ter regions of chemokine receptors, such as CCR1 or CCR2b, with that of CCR5 has been shown to allow virus fusion and entry [19, 26–29]. However, substitution of the N-ter region of CCR5 with that of chemokine receptors CCR1 or CCR2b has not been found to abolish co-receptor activity significantly [19, 26–29], indicating that both regions play important roles in co-receptor activity. Ligand binding and HIV-1 entry are also influenced by the posttranslational sulfation of Y10 and Y14 of the N-ter, which have been shown to bind gp120 at micromolar affinities when included in synthetic peptides [30, 31], contrasted by a complete lack of binding of the non-sulfated forms. Thus, two regions of CCR5 have been postulated to exhibit important functions in cell fusion, the N-ter domain, and the extracellular loops [28]. Transmembrane-spanning domains 4 [32] and 5 [33] have been shown to play a role in co-receptor function, but it is unclear if these domains play a role in direct interaction with gp120, or are important for regulating receptor conformation. A small molecule inhibitor of CCR5 co-receptor function, TAK-779 [34], has been shown to require residues mapped to TM1, 2, 3, and 7 [35]. Other compounds such as SCH-C, SCH-351125, and SCH-350581, as well as members of another set of chemically unrelated small molecule inhibitors, 2-aryl-4-(piperidin-1-yl)butanamines and 1,3,4-trisubstituted pyrrolidines, appear to utilize a non-identical overlapping binding site involving TMs 2, 3, 6, and 7 [36, 37]. Thus, it is likely that these CCR5 antagonists have an allosteric effect on receptor conformation, in contrast to direct blockade of the binding site for physiologic and pathologic ligands.

Three residues in the extracellular domains of CCR5: D11, K171, and K191, have been shown to affect the chemokine binding and co-receptor activity of CCR5 by alanine-scanning mutagenesis [17]. The mutations D11A, K171A, and K191A were found to affect the binding of MIP-1α as well as RANTES, though only the D11A mutation was found to reduce the binding of vMIP-II. CCR5 bearing the D11A mutation was found to display significantly reduced co-receptor activity, while the K171A and K191A mutations were generally less effective in abolishing co-receptor activity [28]. The observed effects of these mutations both on chemokine binding and co-receptor activity are interesting and difficult to rationalize without increased structural information regarding CCR5.

Regions of gp120 postulated to be important for co-receptor binding are near the bridging sheet, formed by a four-stranded, antiparallel β-sheet that includes the variable 1 and 2 (V1/V2) stem and strands (β20 and β21) derived from the fourth conserved gp120 region. This site is adjacent to the variable 3 (V3) loop [38], which is exposed subsequent to CD4 binding. The V3 loop of gp120 has been shown to play important roles in fusion and co-receptor usage by various strains of HIV-1 by viral chimerae [39, 40], recombinant HIV-1 strains [41, 42], and V3 loop chimerae and sequence deletions [43]. This region of gp120 has been shown to be a major determinant of co-receptor specificity [39], and hypothesized to be the molecular basis for HIV-1 phenotypic evolution in vivo. Binding of V3 loop epitopes on gp120 by neutralizing antibodies blocks the interaction of gp120/CD4 complexes with CCR5 [9]. Conserved areas near the V3 loop are important in co-receptor activity [44], and cellular tropism relies on the V3 loop of gp120 [41, 42]. The crown (residues 313 to 327) and the stem regions (residues 303–312 and 328–338) of the V3 loop are both necessary in binding to cell-surface CCR5 [43]. To date, there is no evidence that gp120 can mediate cell fusion without the V3 loop. The various functions attributable to the V3 loop of gp120 make understanding the interactions of this region with CCR5 important in understanding the pathogenesis of HIV-1.

To gain potential insight into the structural mechanisms and distinctions between co-receptor activity and the chemokine-binding regions of CCR5, homology models of the extracellular regions and surrounding transmembrane helices of CCR5, and the alanine mutants D11A, K171A, and K191A were examined by computational modeling and fully solvated restrained molecular dynamics. The effects of these mutations on receptor topology were rationalized by comparison with native CCR5. The V3 loop was docked with CCR5 to construct the functional co-receptor interaction complex of HIV-1. To rationalize the experimental fusion activities of the CCR5 mutants [28] and examine the utility of the model, the V3 loop was docked with the D11A, K171A, and K191A mutants. To further understand the interaction of HIV-1 with a host cell, the global complex consisting of CCR5, gp120 including the V3 loop and CD4 was investigated based upon the experimentally consistent dock of CCR5 with V3.

Materials and methods

The homology model of CCR5 was generated by Modeller4 [45] using an alignment (Omiga, Accelrys, San Diego, CA, USA) with the bovine rhodopsin sequence (accession number P02699) and the rhodopsin crystal structure [46]. Disulfide linkages that have been shown to effect receptor structure and function experimentally were explicitly included at positions C20–C269 and C101–C178 [47]. The extracellular loop regions present in the molecular-dynamics simulations were M1-L36, V83-Y108, P162-L203, and N252-E283. The sulphated residue, Y15, was optimized and parameterized by ab initio calculations using GAMESS [48] with the 6-31G** basis set. The D11A, K171A, and K19A mutants were generated using the homology model, and all simulations underwent the following protocol.

The models were solvated in a 10-Å box of TIP3P water using standard Amber5.0 rules to hydrate the systems and sodium counterions were added randomly for overall charge neutrality. The systems were heated slowly and equilibrated carefully for 125 ps with gradual removal of positional restraints on the protein following this protocol: (1) minimize water, (2) 25 ps MD (T=100 K) holding protein fixed (100 kcal mol^{-1} Å^{-1}), (3) minimize water, (4) minimize total system, (5) 25 ps MD (T=100 K) holding protein fixed (100 kcal mol^{-1} Å^{-1}), (6) 25 ps MD (T=300 K) holding protein fixed (100 kcal mol^{-1} Å^{-1}), (7) 25 ps MD (T=300 K) holding protein fixed (50 kcal mol^{-1} Å^{-1}), (8) 25 ps MD (T=300 K) holding protein fixed (10 kcal mol^{-1} Å^{-1}),(9) 25 ps MD (T=300 K) holding protein fixed (1 kcal mol^{-1} Å^{-1}). Throughout all simulations, including the production phases, the four terminal residues of the transmembrane helices were restrained (750 kcal mol^{-1} Å^{-1}).

Production runs of 4 ns after final equilibrium were used to obtain the average structure (50 snapshots in the last 50 ps), which was fully minimized. Simulations were performed in the isothermic isobaric ensemble (P=1 atm, T=300 K). Periodic boundary conditions and the Particle-Mesh-Ewald algorithm were used. A 1.0-fs time step (4×10^6 steps) was used with bonds involving hydrogen atoms frozen using SHAKE. Molecular-dynamics calculations were carried out with the mpi version of AMBER [49] program sander and parm98.dat parameterization. Calculations were performed on Silicon Graphics Origin 200 servers.

The starting structure of the V3 loop of gp120 was taken from the NMR structure [50] present in the Protein Database, accession number 1CE4. Initial high-resolution docking of the V3 loop with native CCR5 was performed using GRAMM [51]. The matching mode was set to generic, with a grid step of 2.0 Å, grid size of 64 Å, and a 10° angle of rotation. The top 100 matches were output for evaluation. Matches were filtered based upon the following criteria: interaction with the N-ter, ECL2, or both regions of CCR5, a roughly vertical orientation of the V3 loop relative to the receptor, and energy score. The top scoring pose that was consistent with experimental considerations was chosen for optimization via molecular dynamics.

Docking of the V3 loop with receptor mutants was performed by superimposition of the mutant models with the native receptor in the initial docked pose, thus making the docking results uniform for all models. Docked complexes were next subjected to the molecular-dynamics protocol outlined above. The secondary structure of the resultant models was examined using Kabasch–Sander rendering in Insight II. Hydrogen bonding was also examined for average structures via Insight II. Energetic analysis of the trajectory and root-mean-square-difference values were calculated using the AMBER Ptraj module.

The complex of extracellular regions of CCR5, gp120 including the V3 loop, and four extracellular domains of CD4, was created using the final docked model of CCR5 and the V3 loop, with subsequent backbone superimposition of residues Glu276, Ile277, Ile315, and Ser316 of the modeled V3 loop to the crystal structure of gp120 bound to two extracellular domains of CD4 [38]. To provide a more realistic connection to gp120, the truncated base of the V3 loop present in the crystal structure was extended in a β-sheet conformation for residues 277–279 and 313–315. To complete the extracellular regions of CD4, the crystal structure of the four extracellular domains of CD4 [18] was superimposed on the two extracellular domains bound to gp120. The resulting structure was then energy-minimized in a vacuum using the mpi version of the AMBER program Sander and the parm99.dat parameterization.

The complex further underwent implicit solvation via the Generalized Born solvent model, energy minimization, solvent equilibration, and molecular dynamics at 300 K using the standard protocol and parameterization described above. The four terminal residues of the transmembrane helices of CCR5 were restrained (750 kcal mol^{-1} Å^{-1}), while the rest of the complex was unrestrained. Production runs of 700 ps after final equilibrium were used to obtain the average structure (50 snapshots in the last 50 ps), which was fully minimized. The secondary structure of the resultant models was examined using Kabasch–Sander rendering in Insight II. Hydrogen bonding was also examined for average structures via Insight II [46].

Results

Structure of native CCR5

The extracellular regions and surrounding transmembrane helices of CCR5 were stable throughout the 4-ns molecular-dynamics production trajectory and achieved energetic equilibrium within 200 ps (Fig. S1). The base of the representative transmembrane regions were restrained (750 kcal mol^{-1} Å^{-1}) to simulate the positional constraints of the cell membrane, while the rest of the receptor was unrestrained. Sufficient transmembrane helical regions were included to allow for conformational movement of the extracellular regions. The prototypical conformation of the included helical domains remained generally similar to the reported crystal structure of rhodopsin [46]. As expected, the N-ter domain of CCR5 was noted to develop a unique conformation at equilibrium, as did the extracellular loops (Fig. 1). Root-mean-square-difference values (RMSD) were calculated across the production trajectory using the averaged structure as a reference (Fig. 2). This analysis illustrated that the average structure was an accurate representative of the last 2 ns of the trajectory, as well as stable in conformation across the whole trajectory with low RMSDs. The N-ter region containing residues 6–14 of CCR5 was shown to be highly solvent exposed and parallel in orientation relative to the transmembrane axis of the receptor consisting of an antiparallel looped conformation with the turn involving residues 8–12. The N-ter domain also had two regions that formed parallel sheets, residues 1–5 and 15–19, which complete the loop conformation of the N-ter residues 1–19. Charged residues of the N-ter region are noted to form many topologically stabilizing

hydrogen bonds, specifically D2, D11, and E18. The N-ter domain was found to possess partial helical character in residues 18–21, with the side chain of Q21 forming several stabilizing hydrogen bonds.

The N-ter domain was found to make a substantial number of contacts with the extracellular loops. In particular, the base of the N-ter loop, formed by residues 1–5 and 15–19, was found to reside between the solvent-exposed regions of ECL1 and ECL3, thus stabilizing the N-ter. ECL2 plays a critical role in the stability of the N-ter by forming an antiparallel sheet structure from residues 168–180, which acts as a base for N-ter residues 1–5 and 15–19. ECL1 residues 95–99 make close contact with N-ter residues 15–17, with sulfated Y15 hydrogen bonding to T99. Residues 95–99 of ECL1 contact the central sheet portion of ECL2, residues 168–180. ECL2 was found to play two distinctive structural roles in this model, as residues 168–180 form a central platform for the N-ter, while residues 181–192 form a solvent-exposed loop aligned parallel with the main axis of the receptor. ECL2 was shown to contact ECL3, with residues 192–194 of ECL2 in close proximity to residues 253–261 of ECL3. The central portion of ECL2 contacts ECL3, with residue Y176 contacting residue D276 of ECL3. The side chains of ECL3 serve to support the N-ter, with residues 268–274 contacting residues 3–4. The disulfide bond between ECL3 and the N-ter, formed by C269 and C20, is maintained and serves to stabilize the lower portion of the N-ter with respect to ECL3. The most distinctive structural landmarks of the extracellular and surrounding transmembrane domains of CCR5 were found to be two solvent-accessible regions, the N-ter and distal ECL2. The importance of the many charged residues of CCR5 was highlighted, as these residues form many topologically stabilizing hydrogen bonds between different segments of the extracellular domains.

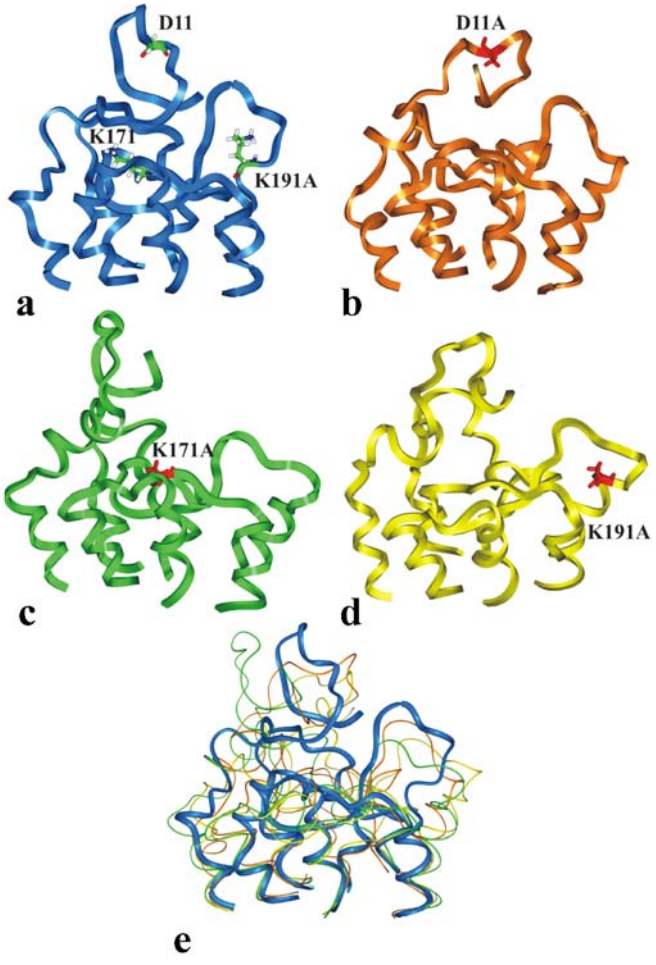

Fig. 1 Structures of extracellular regions of CCR5 and alanine mutants. Averaged structures over the last 50 ps of the 4-ns simulation are shown. **a** CCR5 is shown as a *blue ribbon*, with residues D11, K171, and K191 shown as *stick representation* in atom colors (*red* for oxygen, *green* for carbon, *white* for hydrogen, *purple* for nitrogen) and *labeled*. **b** The CCR5 mutant containing D11A is shown as an *orange ribbon*, with the mutated D11A residue shown as *stick representation* in *red* and *labeled*. **c** CCR5 containing the mutation K171A is shown as a *green ribbon*, with the mutated K171A residue shown as *stick representation* in *red* and *labeled*. **d** The CCR5 mutant containing K191A is shown as a *yellow ribbon*, with the mutated K191A residue shown as *stick representation* in *red* and labeled. **e** Overlay of native CCR5 (*blue ribbon*) and all mutant structures. D11A is presented in *orange ribbon*, K171A in *green ribbon*, and K191A in *yellow ribbon*

Modeling of alanine mutants D11A, K171A, and K191A

Molecular biological experiments have shown that alanine-scanning mutants in positions D11, K171, and K191 have significant effects on physiological and viral chemokine binding to CCR5 [17]. To rationalize the possible changes in CCR5 topology induced by these mutations, these residues were examined for their interactions in the native structure. D11, which formed part of the critical turn of the N-ter, formed four hydrogen bonds with other residues in the N-ter region, (residues S6, S7, and N13) serving to stabilize the conformation of the N-ter. K171 was found to lie in ECL2, forming part of the antiparallel sheet that contacts the N-ter. This residue hydrogen bonded with residues S17 and N98, in the N-ter region and ECL1 respectively, thus serving to stabilize the base of the N-ter and ECL2. K191 is found in ECL2, but in the solvent-exposed loop region, and was found to hydrogen bond with residues T167, Q186, and F189, all of which lie in ECL2. Thus, K191 was found to provide topological stabilization of the solvent-exposed portions of ECL2.

To confirm that the alanine mutants were structurally important, models of CCR5 were created for mutants D11A, K171A, and K191A using the homology model and backbone superimposition of mutant residues. These models were then subjected to the same molecular-dynamics protocols as the native model. All mutants were energetically stable throughout the production trajectory (Figs. S2, S3, S4), and all trajectories were evaluated for stability via RMSD (Figs. S5, S6, S7) from the averaged structures. The mutant that contained D11A was found to differ considerably in conformation from native CCR5

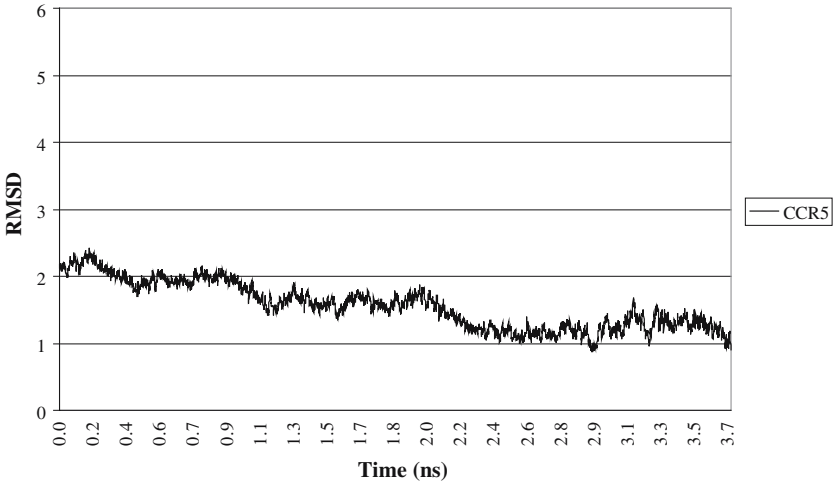

Fig. 2 RMSD of CCR5 across the production trajectory. The RMSD of CCR5 calculated at each Cα position is shown using the final averaged structure as a reference value. RMSD values are plotted on the vertical axis vs time in ns. The conformation of CCR5 was noted to be stable and the averaged structure representative of the conformations present in the production trajectory after 2-ns simulation time

(Fig. 1). This mutation induced changes in the N-ter region, causing reduced interaction between the N-ter region and ECL2, and shortening the N-ter turn to residues 8–10. Unlike the native receptor, in which the N-ter pointed towards ECL2, D11A's N-ter was shifted in the reverse direction, oriented towards ECL3. ECL2 was also found to be different from native, due to a shift of transmembrane helix 5 of approximately 20° from the native position. Residues 88–93 of ECL2 were found to form a more compact conformation than native, making ECL2 less solvent-exposed.

The conformational changes induced by K171A also affected the N-ter and ECL2 regions of CCR5 (Fig. 1). The N-ter was pulled approximately 1–2 Å farther away from ECL2 and orthogonally rotated in position. The N-ter turn consisted of residues P8 and I9. Transmembrane segment 5 was shifted from the native conformation, much like D11A. This was again found to deform ECL2, causing it to be less solvent-exposed than native, involving residues 88–93.

The N-ter of the K191A mutant was found to fold over ECL3, making this region less solvent-exposed (Fig. 1). The characteristic turn of the native N-ter was shortened in this mutant to residues 8–10. The topology of ECL2 differed from the native model, as transmembrane segment 5 was found to be shifted away from the axis of the receptor. Residues 88–92 of ECL2 were more compact, making ECL2 less solvent-exposed.

Complex of native CCR5 with the V3 loop of gp120

The averaged models of the extracellular regions and partial transmembrane helices of CCR5 generated via molecular dynamics were docked with the V3 loop of gp120. Binding of the V3 loop is necessary for CCR5 to function as co-receptor for M-tropic strains of HIV-1, making the understanding of this interaction critical for mechanistic information and drug design. The co-receptor activity [28] of the mutants D11A, K171A, and K191A were rationalized in this manner. CCR5 was docked with the V3 loop using high-resolution docking in GRAMM [51]. The 100 best-scoring docked poses were output for evaluation. Docked poses ranged widely in the placement and orientation of the V3 loop relative to CCR5. These divergent results were evaluated based on criteria derived from previous experimental findings, steric considerations, and energy score. Mutagenesis studies have illustrated the importance of the N-ter and ECL2 regions of CCR5 in co-receptor activity.

Because of these findings, matches were considered for optimization if they demonstrated interaction with one or both of these regions of CCR5. To avoid steric clashes between the receptor and a reconstructed gp120, a roughly vertical orientation of the V3 loop relative to the receptor was assumed to be a requirement. These criteria removed most matches from consideration. Energy score was utilized as a final filter. This evaluation resulted in the fifth docking solution proposed by GRAMM being chosen for further investigation. The four higher scoring results were eliminated by the above criteria. The resultant complex was then refined by undergoing a 4-ns molecular dynamics production run in explicit solvent with the ends of the truncated transmembrane helices restrained (750 kcal mol^{-1} $Å^{-1}$).

The docking position used in the native CCR5 model was replicated for each of the mutant forms of the receptor. This was performed by peptide-backbone superimposition of the mutant models with the native receptor in the initial docked pose. This superimposition ensured minimal variation in the initial position of the V3 loop with reference to CCR5. Because of the structural variation present in the mutant receptors, all docked models were examined for overt steric clashes; however, none were observed. These complexes were then solvated and equilibrated before the production trajectory using an identical protocol.

The complex of native CCR5 and V3 loop of gp120 was energetically stable over the 4-ns molecular-dynamics trajectory (Fig. S8). The V3 loop (residues 303–338 of gp120) interacted with CCR5 from the crown to the helical region, residues 315 to 334 (Fig. 3). Trajectory analysis revealed that the initial docking pose was stable and did not change significantly over the production trajectory (Fig. 4).

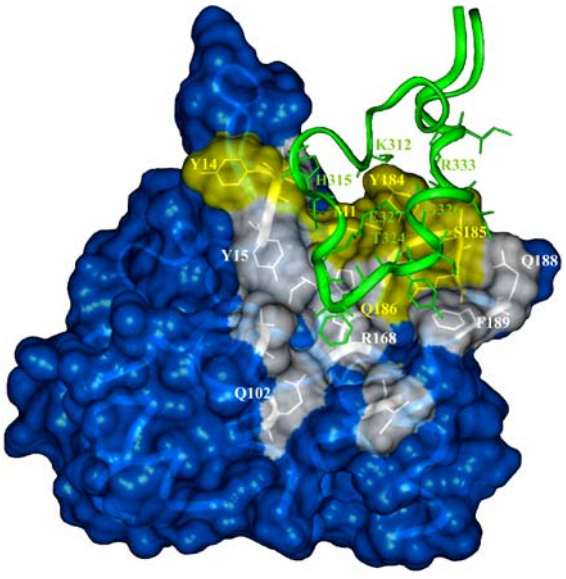

Fig. 3 CCR5 in docked complex with the V3 loop. CCR5 shown in *blue ribbon* with Connelly surfacing. Contact regions of CCR5 are *highlighted* by *stick rendering*, and colored by interaction type, *white* for hydrophobic contacts, *yellow* for electrostatic interactions. The V3 loop is presented in *green ribbon*, with residues interacting with CCR5 *highlighted* by *stick rendering*. Significant residues participating in this interaction are labeled with text *colored* by the above scheme

The first 14 residues of the V3 loop, which are flexible and dynamic, as observed in the NMR structure [50], did not interact significantly with CCR5. The V3 loop formed close contacts at less than 4 Å with N-ter CCR5 residues 1 and 13–15 (Table 1). The extracellular loops formed the majority of the V3 loop-binding region, residues T99 and Q102 of ECL1, and residues I165, R168, H181, and 183–189 of ECL2.

Several residues of ECL2 were found to form a hydrophobic pocket; residues I165, F182, P183, Y184, Y187, F189, and W190, with F189 and W190 displaying stacked aromatic interactions. This region was found to interact with a comparable hydrophobic region of the V3 loop, residues F322, Y323, T324, T325, and G326. R333 of the V3 loop stem was found to exhibit a potential partial π orbital stacking with the aromatic ring of Y184 of CCR5. Hydrogen bonding between CCR5 and the V3 loop in the N-ter and ECL2 regions was observed, from donor to acceptor, M1 of CCR5 to E327 of the V3 loop, G326 of the V3 loop to Q186 of CCR5, and H315 of the V3 loop to Y14 of CCR5 (Table 2).

Significant electrostatic interactions were also observed, pairwise from V3 loop residues to CCR5 residues, K312 to Y184, T324 to M1, and R333 to S185. The V3 loop maintained much of its initial NMR-derived conformation throughout the simulation. The center axis of the V3 loop near its attachment to the rest of gp120 retained its orientation parallel with the transmembrane axis of the receptor, a necessary requirement for this interaction if all of gp120 were present. The stems of the V3 loop, along with the crown region, exhibited critical hydrogen bonds. D331 was found to hydrogen-bond to the amide proton of N307, internally within the V3 loop, which served to anchor the topology of the V3 loop stem regions. R305 was found to serve a similar function by hydrogen-bonding with I328 and D331. K312 formed hydrogen bonds to Q334, which stabilized the topology of both the crown and the helical region of the stem. R320 was found to hydrogen bond to E327, which stabilized the conformation of the crown region of the V3 loop.

Complexes of alanine mutants with the V3 loop of gp120

The docked complex of the CCR5 D11A mutant and V3 loop is consistent with this mutant's reduced co-receptor activity [28]. During the 4-ns molecular-dynamics trajectory, the V3 loop changed position dramatically, with a main axis shift of almost 90° (Fig. 5). Although the complex did reach energetic equilibrium over the production run (Fig. S9), the orientation attained was not feasible, as a complete gp120 molecule could not assume this position due to steric hindrance. This averaged structure was found to be stable and representative of the trajectory after approximately 1.7 ns of the production run (Fig. 6). A significant deviation of 5 Å from the initial docking position was noted, in contrast to the results obtained with the native receptor. This complex illustrated the effect of this mutation on tertiary receptor structure and rationalized the significantly reduced function as a co-receptor [28].

The complex that contained the CCR5 K171A mutant docked with the V3 loop showed many changes from the

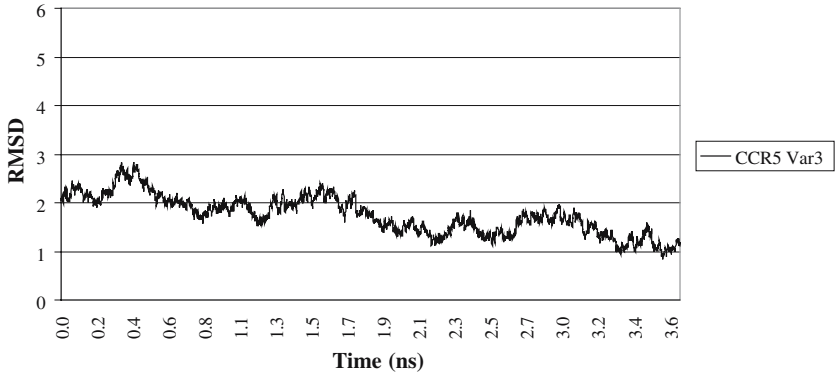

Fig. 4 RMSD analysis of the CCR5/V3 loop complex. The RMSD calculated at the Cα position for both CCR5 and the V3 loop is plotted vs time in ns. The averaged structure was used as a reference value. The docked complex was found to be stable, and the averaged structure was noted to be indicative of the conformations sampled in the production trajectory after 1.9 ns. Overall deviation from the initial docked conformation was found to be relatively minor

Table 1 Close contacts and hydrophobic interactions of CCR5 and the V3 loop

V3 loop	CCR5	Type[a]	Heavy atoms[b]
K312	M1	sc	CE
	Y184	sc	OH
H315	N13	bb	O
	Y14	bb/sc	CA, CB, C, O
	Y15	sc	CB
I316	M1	bb	N
	Y14	bb	O
	Y15	sc	CD1, CE1, OM1
R320	M1	bb	N
A321	Y15	sc	SO, OM1, OM3
	T99	sc	CG2
F322	Y15	sc	SO, OM1, OM2, OM3
	T99	sc	CA, O
	Q102	sc	CD
	I165	bb	O
	R168	sc	CA, CB, CG, CD, NE
Y323	F189	sc	CZ, CE2
T324	M1	bb/sc	N, CA, CB
	R168	sc	CD, NH1
	H181	sc	ND1, CE1
	P183	sc	CG
	Q186	sc	CD, OE1, NE2
	F189	sc	CD1, CE1
T325	Q186	sc	CG, CD, OE1
	F189	sc	CB, CG, CD1, CE1
G326	M1	sc	CG, CD, OE1
	P183	sc	CG, CB
	Y184	bb/sc	CE1, C, O
	Q186	sc	N, CA, CB, CG, CD, OE1
E327	M1	bb	N
I329	S185	bb/sc	CB, OG, C, O
	Q186	bb	CA
	Q188	sc	CD, NE2
G330	Y184	sc	CD1, CE1
	S185	sc	CB, OG
I332	S185	sc	CG
R333	Y184	sc	CB, CG, CD1, CE1, CZ, OH, CE2
	S185	sc	OG

Interactions presented from averaged structure of final 50 ps of 4-ns simulation. Cut off distance for interactions was 4 Å

[a]Interaction type refers to close contacts involving the peptide backbone of the residue (bb) or the side chain (sc)

[b]Heavy atom constituents are specified in standard AMBER nomenclature

Table 2 Hydrogen bonding and electrostatic interactions of CCR5 and the V3 loop

V3 loop	CCR5
Hydrogen bonding	
E327 OE2	M1 N
G326 N	Q186 OE1
H315 NE2	Y14 O
Electrostatic interactions	
K312 NZ	Y184 OH
T324 OG1	M1 N
R333 NE	S185 OG

Interactions presented from averaged structure of final 50 ps of 4-ns simulation. Interactions are shown pair-wise from heavy atom to heavy atom in standard AMBER nomenclature

native complex, although the V3 loop did maintain a bound position over all of the 4-ns trajectory (Fig. 5) and was found to be energetically stable (Fig. S10). RMSD analysis demonstrated that the averaged structure was representative of the trajectory after 2.7 ns of simulation time and stable (Fig. 7). The V3 loop lost some interactions with ECL1 and ECL2, maintaining contact only with residues N98 and Y184, respectively. The V3 loop was found to interact almost exclusively with the N-ter region of CCR5 in this complex, residues 1–2, 8–11, N13, and Y15 at a distance of less than 4 Å. The V3 loop changed conformation over the 4 ns molecular-dynamics trajectory, with a progressive shift of the axis of attachment to gp120 in two orthogonal directions by approximately 30°. The almost planar form of the V3 loop as seen in the native V3 structure was deformed in this docking, with the main axis of the peptide being bent by 90°. The areas of V3 that make contact with K171A are quite different from the native V3 complex, as both sides of the V3 loop, even the flexible first 14 residues, interact with CCR5.

The CCR5 K191A mutant lost contact with the V3 loop during the 4-ns molecular-dynamics trajectory. The simulation was found to be energetically stable throughout the trajectory (Fig. S11). The V3 loop remained in a bound position for 267 ps of the production run, but the interaction between CCR5 and the V3 loop was progressively lost. RMSD analysis of the trajectory revealed a striking divergence between the initial docked structure and the final averaged position, indicating that the complex underwent significant conformational changes leading to the separation of the complex (Fig. 8). To examine this movement in greater detail, RMSD analysis of the V3 loop was performed for this simulation with the initial docked structure as a reference and compared to the results from the native receptor (Fig. 9). This revealed a significant divergence in the position of the V3 loop as the simulation

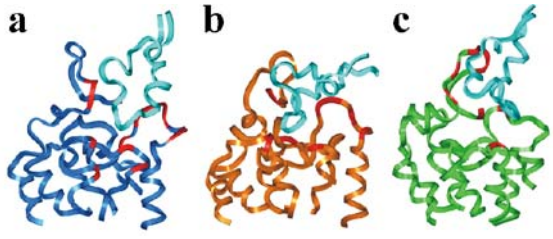

Fig. 5 The V3 loop docking to CCR5 and alanine mutants. Averaged structures over the last 50 ps of the 4-ns simulation are shown; the V3 loop is presented in *cyan*, with residues of each receptor within 4 Å of the V3 loop shown in *red ribbon*. **a** Native CCR5 is shown as a *blue ribbon*. **b** The alanine mutant D11A is shown as an *orange ribbon*. **c** CCR5 containing the mutation K171A is shown as a *green ribbon*

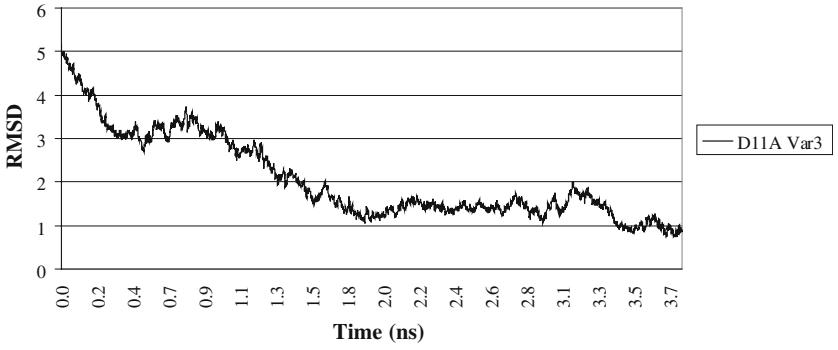

Fig. 6 RMSD analysis of CCR5 mutant D11A/V3 loop complex. The RMSD calculated at the Cα position for both CCR5 and the V3 loop vs time in ns is plotted. The averaged structure was used as a reference for the calculation. This docking result was characterized by an increased deviation from the initial docking conformation, as compared to native CCR5. Although energetically stable, the complex underwent a significant rearrangement of the V3 loop from the initial docked position during the first 1.8 ns of simulation time

progressed. In contrast to the undocked model of the K191A mutant, the N-ter region of this protein was found to possess a vertical orientation relative to the axis of CCR5.

Global complex of CCR5, gp120 and four extracellular domains of CD4

A model of gp120 with the V3 loop, the extracelluar regions of CCR5, and all four extracellular domains of CD4 was constructed based on the docked V3 loop complex with native CCR5. The V3 loop was attached to the crystal structure of the bound gp120/CD4 complex by backbone superimposition of residues surrounding the disulfide formed by C279 and C313. The entire extracellular portion of CD4 was then constructed by superimposing the terminal two extracellular domains complexed with gp120 onto the four-domain crystal structure [18]. The interactions of gp120 and CD4 were identical to the crystal structure. The entire complex was stable over the production run of molecular dynamics at 300 K for 700 ps. Only the four terminal residues of the transmembrane helices of CCR5 were restrained. As expected, the attachment site of the V3 loop was found to be quite flexible, with large conformational shifts possible.

The interactions between gp120 and CD4 were maintained during all of the unrestrained trajectory (Fig. 10). This model shows one possible mode of CCR5 binding via the V3 loop to gp120, with a plausible orientation of CD4. The N-ter region of CCR5 was oriented away from ECL2 towards the transmembrane origin of the N-ter loop. The interactions of gp120 and CCR5 occur mostly via the V3 loop, preserving the interactions of the original model of CCR5 and the V3 loop almost exactly. Significant residues of CCR5 interacting with the V3 loop at a distance of less than 4 Å are residues 14–16 of the N-ter region; T99, M100, and Q102 of ECL1; 164–170, 181–186, and 188–190 of ECL2. Some interactions between CCR5 and gp120 outside of the V3 loop were also present, centered on the interaction between F189 of CCR5 and P437 of gp120, located near the bridging sheet region.

The orientations of all molecules are feasible, with the termination of the extracellular domains of both CD4 and CCR5 lying on the same plane, representative of the cell membrane. In this model, gp120 was found to lie above but offset to the central core of CCR5, at a distance of 3.7 Å in the direction of ECL2. CD4 was found to angle away from the plane of the cell membrane at an angle of approximately 45°, with the distal end making contact with gp120, and the fourth extracellular domain extending behind ECL3. The V1/V2 stem region of gp120 is oriented away

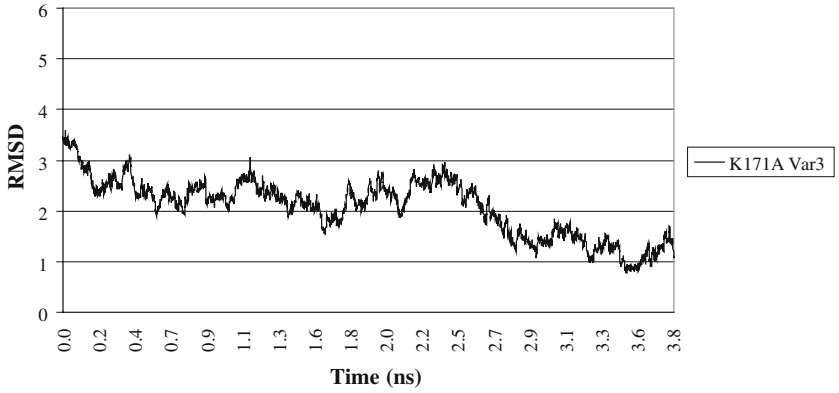

Fig. 7 RMSD analysis of CCR5 mutant K171A/V3 loop complex. The RMSD at the Cα position for both CCR5 and the V3 loop was calculated using the averaged structure as a reference and plotted vs time in ns. The K171A /V3 loop complex was found to be stable, though with a larger divergence from the initial structure than noted with native CCR5

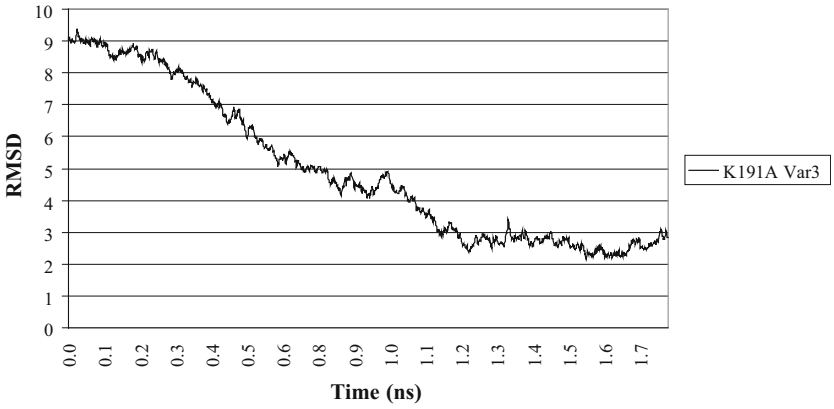

Fig. 8 RMSD analysis of CCR5 mutant K191A/V3 loop complex. The RMSD at the Cα position for both CCR5 and the V3 loop was calculated using the averaged structure as a reference and plotted vs time in ns. The K191A mutant was noted to loose contact with the V3 loop during the production run, resulting in an averaged structure which was quite divergent from the initial binding conformation. This trajectory was found to be characterized by an initial conformational change, which led to a dissociation of the V3 loop from the receptor and was maintained for the remainder of the trajectory

from CCR5 in this model, along a plane formed by the interaction of the bases of ECL2 and ECL3. This model highlights an expanded view of the two-stage model of HIV interaction, illustrating that because of the final orientation of CD4, which must be attained for the complex to interact with CCR5, the CD4/gp120 interaction must take place before co-receptor binding.

To assess the co-receptor-induced conformational change of gp120 during molecular dynamics, the peptide backbone of gp120 was compared with the crystal structure of the gp120/CD4 complex [38]. The root-mean-squared deviation of the peptide backbones of gp120, excluding the V3 loop, as it is not included in the crystal structure, was found to be 3.3 Å. The topology of gp120 was found to be largely conserved, with some conformational changes near the V1/V2 loop stem, which was found to be less solvent exposed, and in residues 213–222, which were more exposed to solvent. The logical continuation of this approach would lead to the reconstruction of gp120/gp41 interactions, to assess conformational changes that lead to the activation of the fusion reaction. Mutation of residues 36–45 and 491–501 of gp120 has been shown to cause

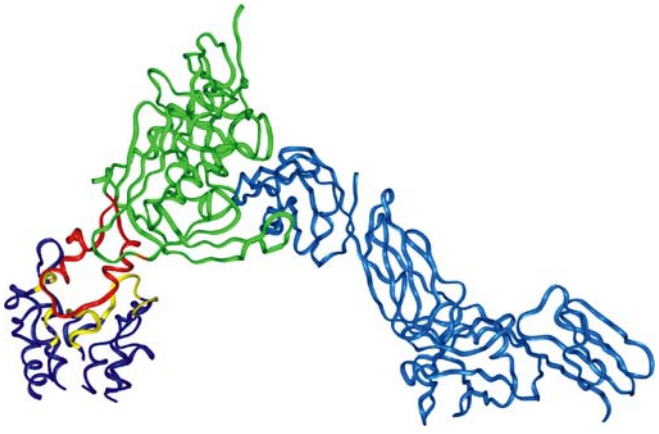

Fig. 10 Complex of CCR5, gp120 including the V3 loop, and the four extracellular domains of CD4. The averaged structure of the complex over the last 50 ps of the 700-ps molecular dynamics simulation is shown. Molecules are shown as *ribbons*, with CCR5 in *blue*, the V3 loop in *red*, gp120 excluding the V3 loop in *green*, and CD4 in *cyan*. Residues of CCR5 within 4 Å of the V3 loop are shown in *yellow ribbon*, while residues of gp120 excluding the V3 loop with 4 Å of CCR5 are shown in *orange ribbon*

Fig. 9 Comparative RMSD analysis of the V3 loop from the native CCR5 simulation vs the mutant K191A. The RMSD at the Cα position of the V3 loops from simulations with native CCR5 (colored *black*) and the K191A (colored *red*) mutant were calculated using the initial docked structure as a reference. The position of the V3 loop was found to diverge from the initial position to a much greater extent when compared to the native simulation. This indicated a greater degree of conformational rearrangement, followed by a loss of binding

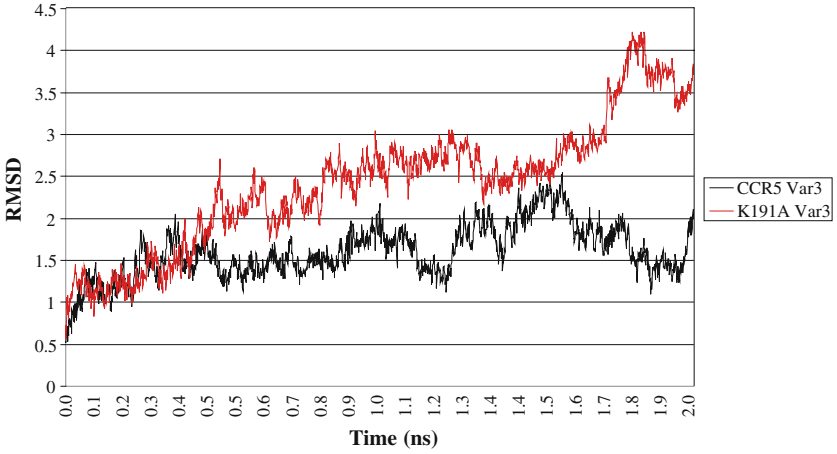

dissociation of envelope glycoprotein subunits [52]. These residues are not present in the crystal structure of the gp120/CD4 complex [38], thus limiting the utility of the crystal structure for this purpose.

Discussion

The models of CCR5 generated in this work were found to provide novel structural insight and rationalization of experimental data that is otherwise unobtainable to date. A fully solvated homology model of the extracellular and partial transmembrane domains of CCR5 was described, using the Particle-Mesh-Ewald summation and periodic boundary conditions. These simulations are unique in the long (4 ns) molecular dynamics trajectories performed, which are necessary for the relaxation of the imposed structure of the extracellular regions based on the starting homology model. The interactions and dynamic nature of the transmembrane domains of CCR5 would not be represented accurately in a fully solvated complete model of CCR5, as the transmembrane regions are highly hydrophobic. Because of this, only the extracellular regions of CCR5 were included, with partial transmembrane helices included as tether points.

The included transmembrane domains of CCR5 maintained a conformation very similar to the rhodopsin crystal structure [46]. The extracellular regions were found to evolve over the course of the molecular-dynamics trajectory, adopting a unique conformation dissimilar to that of rhodopsin. These findings illustrated the importance of molecular dynamics in the refinement of homology models, as the constrained initial model was permitted to relax and assume the conformation of CCR5. The N-ter region was found to adopt a loop conformation unlike that of the rhodopsin crystal structure, which resided above the proximal sheet portion of ECL2. The larger size of ECL2, as compared to rhodopsin, was noted to produce another unique feature of CCR5, a solvent-exposed loop aligned parallel to the main axis of the receptor. CCR5 was found to exhibit two major solvent-exposed regions, the N-ter region and a distal loop portion of ECL2 (residues 181–192). These regions have been shown to be critical for envelope-mediated fusion [28], as well as chemokine binding [17], and are accessible in this model.

The complex of gp120/CCR5/CD4 has been modeled previously [53, 54]. These studies utilized LOOP SEARCH algorithms for generating the extracellular domains of CCR5, neglecting much of the information present in the only available crystal structure of a GPCR [46]. It is unclear as to whether these computational strategies [55, 56] can predict, ab initio, the structure of rhodopsin itself accurately. However, a recent report shows that the structure of rhodopsin can be generated from first principles [57]. Previous modeling studies of CCR5 designed to rationalize the binding of inhibitors to the transmembrane domains of CCR5 were performed via a combination of homology modeling and simulated annealing followed by molecular dynamics in vacuo [58]. Several differences are apparent in the models previously used for CCR5 and our model. The most striking of these differences involve the conformation of the N-ter region and ECL2, two domains critical to co-receptor function. The previous models of CCR5 have significantly different interhelical loop regions, both from each other and our model based on the rhodopsin crystal structure. One previously generated model of the interactions between CCR5 and gp120 neglected to include the V3 loop [53], despite the critical importance of this region for co-receptor function. Another model [54] of this complex did include the V3 loop, but it was added after the initial placement of gp120. The relative positions of gp120 and CCR5 in that model were dictated by the position of the 17b antibody present in the crystal structure [38]. The starting structures and methodologies used in this study are unique in that they were based on a complete homology model derived from the rhodopsin crystal structure, including the essential V3 loop of gp120 based on the available NMR structure [50], and consist of fully solvated molecular-dynamics trajectories of a long time scale (4 ns) necessary to relax the starting structures and provide conformational flexibility to the complex. Similar methodology has been shown to be effective in rationalizing experimental data in other chemokine receptor systems [59].

A stable complex of the V3 loop of gp120 and native CCR5 is presented here, centered on interactions with ECL2 and the N-ter region of CCR5, as is supported by molecular biological data [17, 43]. This complex provides an overall binding model in which the crown and helical stem of the V3 loop interact directly with CCR5. The GPG motif of the V3 loop has been shown to play an important role in CCR5 binding [60] by alanine mutagenesis, purportedly due to the induction of topological changes in the crown region of the V3 loop.

In this study, the crown region forms many interactions with CCR5, with continual interaction from V3 loop residues R320 to E327. Disruption of this would severely impact the ability of the V3 loop to bind CCR5, as observed experimentally [40, 43, 60–62]. The V3 crown region has been shown to determine the specificity of co-receptor usage [43], and experimental evidence indicates this interaction is reliant upon the loops of CCR5 [61]. Important residues for V3 loop interaction with cell surface CCR5, as well as sulfated peptides derived from the N-ter region, have been localized to the crown and stem regions of the V3 loop [43, 61] by alanine-scanning mutagenesis. These results are supported, as the crown region is shown to form many interactions with ECL2, both via electrostatic and hydrophobic effects.

The stem regions of the V3 loop are shown to play two important functions in this model, serving to anchor the topology of the V3 loop as well as making direct contacts with CCR5 at residues K312, 329–330, and 332–333. These results rationalize the importance attached to these regions by mutagenesis data [43, 61]. Residues R305 and N307, purported to be critical in binding to CCR5 [61, 63], were shown in this complex to play a role in stabilizing the topology of the V3 loop by hydrogen-bonding to I328 and

D331, which were likewise found to play important roles in binding to CCR5 [61, 64]. The importance of R320 and F322 of the crown region of the V3 loop of gp120 has been shown in several reports [61, 62].

In the presented complex, this is rationalized both by direct interaction with CCR5, as well as topologically. R320 formed a hydrogen bond with E327 of the stem region of CCR5, anchoring the topology of the crown region. F322 interacted with a hydrophobic pocket on CCR5, thus contributing directly to the interaction of the V3 loop and CCR5. The helical half of the V3 loop is sufficient to confer the ability to infect CCR5-expressing cells to HXB2, a strain that, when unaltered, shows X4 viral tropism [40]. The simulations presented in this paper support these findings, as this region of the V3 loop is the primary site of interaction with CCR5.

Additional information regarding the interaction of the V3 loop with CCR5 can be obtained from structural studies of inhibitors of this interaction, such as the small molecules SCH-351125, SCH-350581, and TAK-779, whose interactions with CCR5 have been examined previously [35, 36]. These compounds' interactions with CCR5 have been mapped to the transmembrane domains of the receptor, in a cavity formed by transmembrane helices 1, 2, 3, and 7 [35, 36]. The proposed mode of action of these compounds is disruption of the topology of the extracellular loops [35, 36, 65], which is supported in the case of the SCH compounds by their ability to block antibodies specific to ECL2 [36]. In our CCR5 model, the residues that were found critical to the interaction of these compounds are located in the transmembrane region just below the antiparallel sheet formed by residues 168–180 of ECL2. Due to this close proximity, binding of these residues by small molecule inhibitors could easily change the topology of ECL2, alter the V3 binding site proposed in this paper, and inhibit gp120 interaction, in agreement with experimental results.

To rationalize experimental data further and validate the proposed model, three alanine-scanning mutants for which biological data is available [17, 28] were examined. The mutant D11A was found to be disordered in the N-ter region and ECL2 of CCR5, which explains its lack of activity in binding RANTES, MIP-1α and vMIP-II [17], which were shown to utilize these regions. The dramatic topological effects of this mutation, in combination with the loss of ability to bind the V3 loop in an effective conformation, also explain the decreased co-receptor activity associated with this mutant [28]. The mutant model containing K171A had its most dramatic effect on the topology of ECL2. This rationalizes the finding that this mutant had decreased chemokine binding affinity for RANTES and MIP-1α [17]. This mutant's relative sparing of N-ter topology supports the near-native levels of interaction with vMIP-II. The complex of K171A and the V3 loop of gp120 was stable, albeit deformed from native.

This explains this mutant's continued ability to act as a co-receptor for HIV-1 [28], as the flexibility of the V3 loop may be able to compensate somewhat for the topological changes of this mutant. The K191A mutant was found to affect the conformation of ECL2, and to destabilize the tertiary structure of the N-ter region. These topological changes in the extracellular loops rationalize this mutant's reduced chemokine binding [17]. The complex of K191A with the V3 loop was unstable over the course of the 4-ns trajectory, although the interaction was maintained for roughly 267 ps of unrestrained simulation time. This instability seems paradoxical, as this mutant was found to exhibit fusion activity [28]. One possible explanation could be that the topological changes induced by the K191A mutation are able to reduce the affinity of the V3 loop for CCR5, though not enough to abolish co-receptor activity.

One striking structural feature noted in CCR5 is the conformational interdependence of the extracellular domains. As suggested by the simulations involving the alanine mutants of CCR5, charged residues in the N-ter and ECL regions form topologically stabilizing hydrogen bonds, which tie these domains together. Thus, mutations in these positions would yield conformational instability, and can explain the findings of reduced chemokine binding or co-receptor activity from molecular biology. The two major solvent-exposed regions of CCR5, the N-ter and ECL2, are seen to play important binding roles in the interaction with the V3 loop, which is consistent with previous information.

Other residues that do not directly participate in binding the V3 loop generally stabilize the structure of CCR5, without which co-receptor recognition would be impaired. The models presented in this work focus on the extracellular regions of CCR5, with inclusion of enough transmembrane segments to allow conformational flexibility. Because of this, ligand-binding information and co-receptor function could be investigated. For mechanistic information to be gained regarding CCR5 signaling and co-receptor activity, molecular-dynamics simulations of a full homology model in a lipid bilayer environment will be necessary, as has been done with the related chemokine receptor CXCR4 [59].

The models presented in this paper help to define the specific interactions between the V3 loop of gp120 and CCR5, the functional unit of co-receptor activity. This interaction is particularly critical to our understanding of cell fusion because of the ability of the V3 loop to provide co-receptor specificity [39]. The structural understanding provided in this paper could be used further to orient and study the global CCR5–gp120–CD4 complex. These insights are unobtainable by more traditional methods due to the recalcitrant nature of membrane proteins, demonstrating that the combination of molecular modeling with molecular biological data is a powerful tool allowing advances in our understanding of these interactions. We have identified possible key residues of the N-ter region and ECL2 of CCR5 for co-receptor activity and chemokine binding. The interactions between the V3 loop of gp120 and CCR5 are illustrated.

The topological changes induced by mutations in these regions successfully rationalize the molecular biological data previously obtained for chemokine binding and co-receptor activity [60]. The models presented successfully

rationalize the mutagenesis data reported to date for the V3 loop of gp120, as well as give support to previous reports studying inhibitor binding sites [30, 35, 36, 61]. A plausible structure of the global complex of HIV-1 cell surface interaction is presented that satisfies known experimental constraints. These findings provide specific information and predictive ability usable for new directions that may be investigated. The structural understanding of these relationships is essential to any rational approach to drug design combating the use of CCR5 as a co-receptor by HIV-1, and may guide the design of novel inhibitors.

Acknowledgement SCP acknowledges financial support from the National Institutes of Health (5R01AI041346-07).

References

1. Samson M, Labbe O, Mollereau C, Vassart G, Parmentier M (1996) Biochemistry 35:3362–3367
2. Lee B, Sharron M, Montaner LJ, Weissman D, Doms RW (1999) Proc Natl Acad Sci USA 96:5215–5220
3. Bonecchi R, Bianchi G, Bordignon PP, D'Ambrosio D, Lang R, Borsatti A, Sozzani S, Allavena P, Gray PA, Mantovani A, Sinigaglia F (1998) J Exp Med 187:129–134
4. Sallusto F, Lenig D, Mackay CR, Lanzavecchia A (1998) J Exp Med 187:875–883
5. Connor RI, Mohri H, Cao Y, Ho DD (1993) J Virol 67: 1772–1777
6. Schuitemaker H, Koot M, Kootstra NA, Dercksen MW, de Goede RE, van Steenwijk RP, Lange JM, Schattenkerk JK, Miedema F, Tersmette M (1992) J Virol 66:1354–1360
7. Alkhatib G, Combadiere C, Broder CC, Feng Y, Kennedy PE, Murphy PM, Berger EA (1996) Science 272:1955–1958
8. Trkola A, Dragic T, Arthos J, Binley JM, Olson WC, Allaway GP, Cheng-Mayer C, Robinson J, Maddon PJ, Moore JP (1996) Nature 384:184–187
9. Wu L, Gerard NP, Wyatt R, Choe H, Parolin C, Ruffing N, Borsetti A, Cardoso AA, Desjardin E, Newman W, Gerard C, Sodroski J (1996) Nature 384:179–183
10. Samson M, Libert F, Doranz BJ, Rucker J, Liesnard C, Farber CM, Saragosti S, Lapoumeroulie C, Cognaux J, Forceille C, Muyldermans G, Verhofstede C, Burtonboy G, Georges M, Imai T, Rana S, Yi Y, Smyth RJ, Collman RG, Doms RW, Vassart G, Parmentier M (1996) Nature 382:722–725
11. Liu R, Paxton WA, Choe S, Ceradini D, Martin SR, Horuk R, MacDonald ME, Stuhlmann H, Koup RA, Landau NR (1996) Cell 86:367–377
12. Deng H, Liu R, Ellmeier W, Choe S, Unutmaz D, Burkhart M, Di Marzio P, Marmon S, Sutton RE, Hill CM, Davis CB, Peiper SC, Schall TJ, Littman DR, Landau NR (1996) Nature 381:661–666
13. Cocchi F, DeVico AL, Garzino-Demo A, Arya SK, Gallo RC, Lusso P (1995) Science 270:1811–1815
14. Jansson M, Popovic M, Karlsson A, Cocchi F, Rossi P, Albert J, Wigzell H (1996) Proc Natl Acad Sci USA 93:15382–15387
15. Moore PS, Boshoff C, Weiss RA, Chang Y (1996) Science 274:1739–1744
16. Boshoff C, Endo Y, Collins PD, Takeuchi Y, Reeves JD, Schweickart VL, Siani MA, Sasaki T, Williams TJ, Gray PW, Moore PS, Chang Y, Weiss RA (1997) Science 278:290–294
17. Navenot JM, Wang ZX, Trent JO, Murray JL, Hu QX, DeLeeuw L, Moore PS, Chang Y, Peiper SC (2001) J Mol Biol 313:1181–1193
18. Wu H, Kwong PD, Hendrickson WA (1997) Nature 387: 527–530
19. Rucker J, Samson M, Doranz BJ, Libert F, Berson JF, Yi Y, Smyth RJ, Collman RG, Broder CC, Vassart G, Doms RW, Parmentier M (1996) Cell 87:437–446
20. Agrawal L, Van Horn-Ali Z, Berger EA, Alkhatib GA (2004) Blood 103:1211–1217
21. Lee B, Sharron M, Blanpain C, Doranz BJ, Vakili J, Setoh P, Berg E, Liu G, Guy HR, Durell SR, Parmentier M, Chang CN, Price K, Tsang M, Doms RW (1999) J Biol Chem 274: 9617–9626
22. Olson WC, Rabut GE, Nagashima KA, Tran DN, Anselma DJ, Monard SP, Segal JP, Thompson DA, Kajumo F, Guo Y, Moore JP, Maddon PJ, Dragic T (1999) J Virol 73:4145–4155
23. Blanpain C, Doranz BJ, Vakili J, Rucker J, Govaerts C, Baik SS, Lorthioir O, Migeotte I, Libert F, Baleux F, Vassart G, Doms RW, Parmentier M (1999) J Biol Chem 274: 34719–34727
24. Dragic T, Trkola A, Lin SW, Nagashima KA, Kajumo F, Zhao L, Olson WC, Wu L, Mackay CR, Allaway GP, Sakmar TP, Moore JP, Maddon PJ (1998) J Virol 72:279–285
25. Farzan M, Choe H, Vaca L, Martin K, Sun Y, Desjardins E, Ruffing N, Wu L, Wyatt R, Gerard N, Gerard C, Sodroski J (1998) J Virol 72:1160–1164
26. Atchison RE, Gosling J, Monteclaro FS, Franci C, Digilio L, Charo IF, Goldsmith MA (1996) Science 274:1924–1926
27. Bieniasz PD, Fridell RA, Aramori I, Ferguson SS, Caron MG, Cullen BR (1997) EMBO J 16:2599–2609
28. Doranz BJ, Lu ZH, Rucker J, Zhang TY, Sharron M, Cen YH, Wang ZX, Guo HH, Du JG, Accavitti MA, Doms RW, Peiper SC (1997) J Virol 71:6305–6314
29. Picard L, Simmons G, Power CA, Meyer A, Weiss RA, Clapham PR (1997) J Virol 71:5003–5011
30. Cormier EG, Persuh M, Thompson DA, Lin SW, Sakmar TP, Olson WC, Dragic T (2000) Proc Natl Acad Sci USA 97: 5762–5767
31. Farzan M, Vasilieva N, Schnitzler CE, Chung S, Robinson J, Gerard NP, Gerard C, Choe H, Sodroski J (2000) J Biol Chem 275:33516–33521
32. Siciliano SJ, Kuhmann SE, Weng Y, Madani N, Springer MS, Lineberger JE, Danzeisen R, Miller MD, Kavanaugh MP, DeMartino JA, Kabat D (1999) J Biol Chem 274:1905–1913
33. Wang Z, Lee B, Murray JL, Bonneau F, Sun Y, Schweickart V, Zhang T, Peiper SC (1999) J Biol Chem 274:28413–28419
34. Baba M, Nishimura O, Kanzaki N, Okamoto M, Sawada H, Iizawa Y, Shiraishi M, Aramaki Y, Okonogi K, Ogawa Y, Meguro K, Fujino M (1999) Proc Natl Acad Sci USA 96: 5698–5703
35. Dragic T, Trkola A, Thompson DA, Cormier EG, Kajumo FA, Maxwell E, Lin SW, Ying W, Smith SO, Sakmar TP, Moore JP (2000) Proc Natl Acad Sci USA 97:5639–5644
36. Tsamis F, Gavrilov S, Kajumo F, Seibert C, Kuhmann S, Ketas T, Trkola A, Palani A, Clader JW, Tagat JR, McCombie S, Baroudy B, Moore JP, Sakmar TP, Dragic T (2003) J Virol 77:5201–5208
37. Castonguay LA, Weng Y, Adolfsen W, Di Salvo J, Kilburn R, Caldwell CG, Daugherty BL, Finke PE, Hale JJ, Lynch CL, Mills SG, MacCoss M, Springer MS, DeMartino JA (2003) Biochemistry 42:1544–1550
38. Kwong PD, Wyatt R, Robinson J, Sweet RW, Sodroski J, Hendrickson WA (1998) Nature 393:648–659
39. Speck RF, Wehrly K, Platt EJ, Atchison RE, Charo IF, Kabat D, Chesebro B, Goldsmith MA (1997) J Virol 71:7136–7139
40. Hung CS, Vander Heyden N, Ratner L (1999) J Virol 73: 8216–8226
41. Cann AJ, Churcher MJ, Boyd M, O'Brien W, Zhao JQ, Zack J, Chen IS (1992) J Virol 66:305–309
42. Hwang SS, Boyle TJ, Lyerly HK, Cullen BR (1991) Science 253:71–74
43. Cormier EG, Dragic T (2002) J Virol 76:8953–8957
44. Rizzuto CD, Wyatt R, Hernandez-Ramos N, Sun Y, Kwong PD, Hendrickson WA, Sodroski J (1998) Science 280:1949–1953
45. Sali A, Blundell TL (1990) J Mol Biol 212:403–428

46. Palczewski K, Kumasaka T, Hori T, Behnke CA, Motoshima H, Fox BA, Le Trong I, Teller DC, Okada T, Stenkamp RE, Yamamoto M, Miyano M (2000) Science 289:739–745
47. Blanpain C, Lee B, Vakili J, Doranz BJ, Govaerts C, Migeotte I, Sharron M, Dupriez V, Vassart G, Doms RW, Parmentier M (1999) J Biol Chem 274:18902–18908
48. Schmidt MW, Baldridge KK, Boatz JA, Elbert ST, Gordon MS, Jensen JJ, Koseki S, Matsunaga N, Nguyen KA, Su S, Windus TL, Dupuis M, Montgomery JA (1993) J Comput Chem 14:1347–1363
49. Cornell WD, Cieplak P, Bayly CI, Gould IR, Merz KM, Ferguson DM, Spellmeyer DC, Fox T, Caldwell JW, Kollman PA (1995) J Am Chem Soc 117:5179–5197
50. Vranken WF, Budesinsky M, Fant F, Boulez K, Borremans FA (1995) FEBS Lett 374:117–121
51. Katchalski-Katzir E, Shariv I, Eisenstein M, Friesem AA, Aflalo C, Vakser IA (1992) Proc Natl Acad Sci USA 89: 2195–2199
52. Helseth E, Olshevsky U, Furman C, Sodroski J (1991) J Virol 65:2119–2123
53. Liu S, Fan S, Sun Z (2003) J Mol Model (Online)
54. Yang J, Liu CQ (2000) Acta Pharmacol Sin 21:29–34
55. Zhou N, Luo Z, Luo J, Liu D, Hall JW, Pomerantz RJ, Huang Z (2001) J Biol Chem 276:42826–42833
56. Huang X, Shen J, Cui M, Shen L, Luo X, Ling K, Pei G, Jiang H, Chen K (2003) Biophys J 84:171–184
57. Vaidehi N, Floriano WB, Trabanino R, Hall SE, Freddolino P, Choi EJ, Zamanakos G, Goddard WA III (2002) Proc Natl Acad Sci USA 99:12622–12627
58. Paterlini MG (2002) Biophys J 83:3012–3031
59. Trent JO, Wang ZX, Murray JL, Shao W, Tamamura H, Fujii N, Peiper SC (2003) J Biol Chem 278:47136–47144
60. Hu Q, Trent JO, Tomaras GD, Wang Z, Murray JL, Conolly SM, Navenot JM, Barry AP, Greenberg ML, Peiper SC (2000) J Mol Biol 302:359–375
61. Cormier EG, Tran DN, Yukhayeva L, Olson WC, Dragic T (2001) J Virol 75:5541–5549
62. Wang WK, Dudek T, Essex M, Lee TH (1999) Proc Natl Acad Sci USA 96:4558–4562
63. Wang WK, Dudek T, Zhao YJ, Brumblay HG, Essex M, Lee TH (1998) Proc Natl Acad Sci USA 95:5740–5745
64. Hu Q, Napier KB, Trent JO, Wang Z, Taylor S, Griffin GE, Peiper SC, Shattock RJ (2005) J Mol Biol 350:699–712
65. Billick E, Seibert C, Pugach P, Ketas T, Trkola A, Endres MJ, Murgolo NJ, Coates E, Reyes GR, Baroudy BM, Sakmar TP, Moore JP, Kuhmann SE (2004) J Virol 78:4134–4144